THE JOURNAL OF PHYSICAL CHEMISTRY B LETTERS

2006, *110,* 18097−18103
Published on Web 08/25/2006

Femtosecond Studies of Tryptophan Fluorescence Dynamics in Proteins: Local Solvation and Electronic Quenching

Luyuan Zhang, Ya-Ting Kao, Weihong Qiu, Lijuan Wang, and Dongping Zhong*

Departments of Physics, Chemistry, and Biochemistry, Programs of Biophysics, Chemical Physics, and Biochemistry, 191 West Woodruff Avenue, The Ohio State University, Columbus, Ohio 43210

Received: May 17, 2006; In Final Form: July 19, 2006

We report our systematic examination of tryptophan fluorescence dynamics in proteins with femtosecond resolution. Distinct patterns of femtosecond-resolved fluorescence transients from the blue to the red side of emission have been characterized to distinguish local ultrafast solvation and electronic quenching. It is shown that tryptophan is an ideal local optical probe for hydration dynamics and protein−water interactions as well as an excellent local molecular reporter for ultrafast electron transfer in proteins, as demonstrated by a series of biological systems, here in melittin, human serum albumin, and human thioredoxin, and at lipid interfaces. These studies clarify the assignments in the literature about the ultrafast solvation or quenching dynamics of tryptophan in proteins. We also report a new observation of solvation dynamics at far red-side emission when the relaxation of the local environment is slower than 1 ps. These results provide a molecular basis for using tryptophan as a local molecular probe for ultrafast protein dynamics in general.

I. Introduction

Tryptophan (Trp or W), the most important fluorophore among amino acids, has been extensively used for decades to study protein dynamics by measuring changes in its emission maximum and width, quantum yield, lifetime, and time-resolved anisotropy,[1−6] as well as widely utilized as an electron or energy donor for studies of electron transfer or resonance energy transfer in proteins.[7−11] The first two singlet excited states (^1L_a and ^1L_b) are nearly degenerate. In a polar environment, the observed fluorescence is dominant from the ^1L_a state due to its larger static dipole moment and the internal conversion of ^1L_b to ^1L_a occurs ultrafast in less than 100 fs.[11,12] Because of its conformational flexibility and amino- and carboxyl-quenching groups in proximity, the ^1L_a state has at least two distinct lifetimes (500 ps and 3 ns) due to proton and electron transfer reactions (Scheme 1).[13] In proteins, depending on local structural integrity, the excited state could be quenched by neighboring peptide bonds and other amino acid residues (Scheme 1), resulting in multiple lifetimes.[1−4]

The recent renaissance in studies of tryptophan in proteins revealed that in the time window from femtosecond to subnanosecond (0.1−500 ps) tryptophan is an ideal optical probe for hydration dynamics and protein−water interactions,[11,14−19] a long-standing issue in protein hydration.[20−28] This time window covers the dynamical range of water motions around proteins. By monitoring the fluorescence Stokes shifts with time, one can obtain the local solvation dynamics around tryptophan residue. We have recently developed a method to extract pure dynamical Stokes shifts from the overall spectrum shifts by the careful consideration of heterogeneous lifetime emissions (decay-associated emission spectra).[16−18]

SCHEME 1

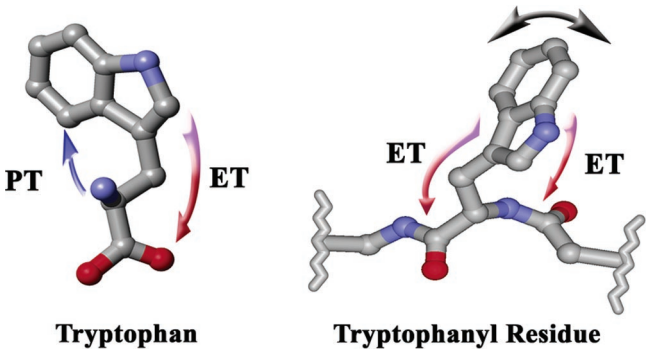

We have used tryptophan as a local optical probe to scan a protein surface using site-directed mutagenesis and to map out the global hydration dynamics around a protein.[29] We carefully designed and screened tryptophan mutants and selected unquenched ones as local molecular probes. In this letter, we report the femtosecond- and wavelength-resolved fluorescence transients and their various patterns from the blue to the red side of tryptophan emission under different local environments from numerous systems we have studied. These studies clarify the assignments in the literature about the dynamics of ultrafast local solvation and electronic quenching.[30] We also report a new observation of red-side solvation when the relaxation of local environments is slower than the excited wave packet spreading. These results provide a molecular basis for using Trp as a local molecular probe for studies of ultrafast protein dynamics in general.

II. Experimental Section

The experimental setup is schematically shown in Figure 1, including both fluorescence up-conversion and high-sensitive

* Corresponding author. Phone: (614)292-3044. Fax: (614)292-7557. E-mail: dongping@mps.ohio-state.edu.

10.1021/jp063025e CCC: $33.50

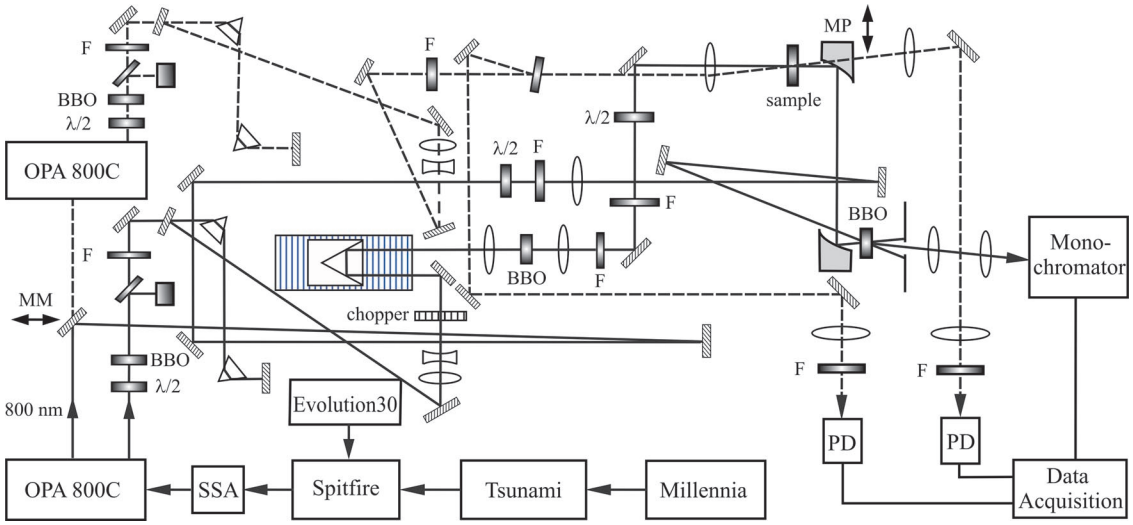

Figure 1. Schematic representation of the experimental setup with both fluorescence up-conversion and transient-absorption configurations. The dashed line is for the transient-absorption probe pathway. F, filter. MM, movable mirror. MP, movable parabolic mirror. PD, photodiode.

transient absorption methods. Most experimental measurements were carried out by the femtosecond-resolved fluorescence up-conversion technique. Briefly, a femtosecond pulse at 580 (or 590) nm, produced from an optical parametric amplifier system (OPA-800C, Spectra-Physics), was frequency-doubled to generate our pump wavelength at 290 (or 295) nm by a 0.2-mm-thick BBO crystal. The pump pulse energy was typically attenuated to ~140 nJ prior to being focused into the motor-controlled moving sample cell. The fluorescence emission was collected by a pair of parabolic mirrors and mixed with a gating pulse (800 nm) in another 0.2-mm BBO crystal through a noncollinear configuration. The up-converted signal ranging from 218 to 292 nm was detected. The instrument response time under the current noncollinear geometry is between 400 and 500 fs as determined from the up-conversion signal of Raman scattering by water at around 320 nm. For transient absorption measurements, we remove two movable mirrors (MM and MP in Figure 1) out of the beam pathways to achieve a quick switch between the two techniques. Various probe wavelengths were generated from the second OPA system. The resulting response time for transient absorption is about 140 fs. All measurements were carried out at the magic-angle (54.7°) condition.

The sample preparation and experimental conditions of melittin,[18] human serum albumin,[19] human thioredoxin,[31] and various lipid solutions[32] have been described elsewhere. All proteins reported here contain only a single tryptophan residue, and their steady-state fluorescence emissions were characterized using a SPEX FluoroMax-3 spectrometer. Typically, the emission maximum of tryptophan in proteins ranges from 308 nm (hydrophobic) to 350 nm (fully water-exposed), and the peak position is a direct indicator of local polarity around tryptophan.

III. Results and Discussion

A. Ultrafast Solvation Dynamics. Figure 2a shows the fluorescence emission of melittin, a 26 amino acid peptide, in water at pH 4 in a random-coiled form with the peak at 348.5 nm, indicating a great exposure of intrinsic Trp19 to an aqueous environment. A series of femtosecond-resolved fluorescence up-conversion transients from the blue to the red side are shown in Figure 2b. At the blue side of the peak emission, all transients exhibit ultrafast decay dynamics with two solvation components in 0.4−1.3 and 4.4−25 ps, systematically slowing down from 305 nm to the emission peak (348.5 nm). At the red side, we observed two initial rise components in all transients with the time scales of ~0.24 and 1.8−4.2 ps. The initial rise time scale at ~440 nm is similar to the ultrafast decay at ~305 nm. Besides two long-lifetime emissions, we did not observe any fast decay component in all red-side transients. Thus, there is no any fast-quenching dynamics of Trp19 in melittin. In the *entire* emission range, the long-lifetime contributions systematically increase from the blue to the red side, consistent with the decay-associated emission spectra (DAS).[33] The observed transient pattern, decay at the blue side and rise at the red side, is a typical signature of solvation dynamics (vibrational relaxation has been carefully examined and excluded).[18] Using the method we developed,[16] we obtained the local solvation dynamics around Trp19 in a biphasic distribution of 0.62 ps (68% amplitude) and 14.7 ps (32%).[18] These two time scales truly represent the local solvation response around Trp19 of the random-coiled melittin monomer in water.

Under high-salt conditions, melittin aggregates to form a tetramer. The emission peak shifts to the blue at 333.5 nm, indicating a more hydrophobic location of Trp19 in the tetramer as also observed by the X-ray structure.[34] The gated fluorescence transients show a similar pattern from 305 nm at the blue side to 380 nm at the red side, but with significantly slow solvation dynamics (Figure 2c). Similarly, at the blue side, the two solvation components decay in 2−10 and 30−100 ps, systematically slowing down from 305 nm to the emission peak (333.5 nm). At the red side from 335 to 380 nm, we also observed two initial rise components in all transients with the time scales of ~0.5 and 5 ps, together with a systematical increase of long-lifetime contributions. We did not observe any picosecond decay component in the range 335−380 nm at the red-side emission. Instead, we observed systematic picosecond rise components, corresponding to the blue-side decay, reflecting the slow solvation dynamics of Trp19 in melittin tetramer. Similarly, we obtained the local solvation dynamics around Trp19 in a biphasic distribution of 3 ps (47% amplitude) and 87 ps (53%).[18] These two time scales represent the local solvation processes, not quenching dynamics, around Trp19 in melittin tetramer in buffer solution. Both time scales are significantly slower than those obtained for the random-coiled monomer, and the first solvation dynamics (3 ps) has extended to longer than 1 ps.

When we gated the fluorescence emission at the far-red side, such as at 440 nm, we observed an ultrafast decay component

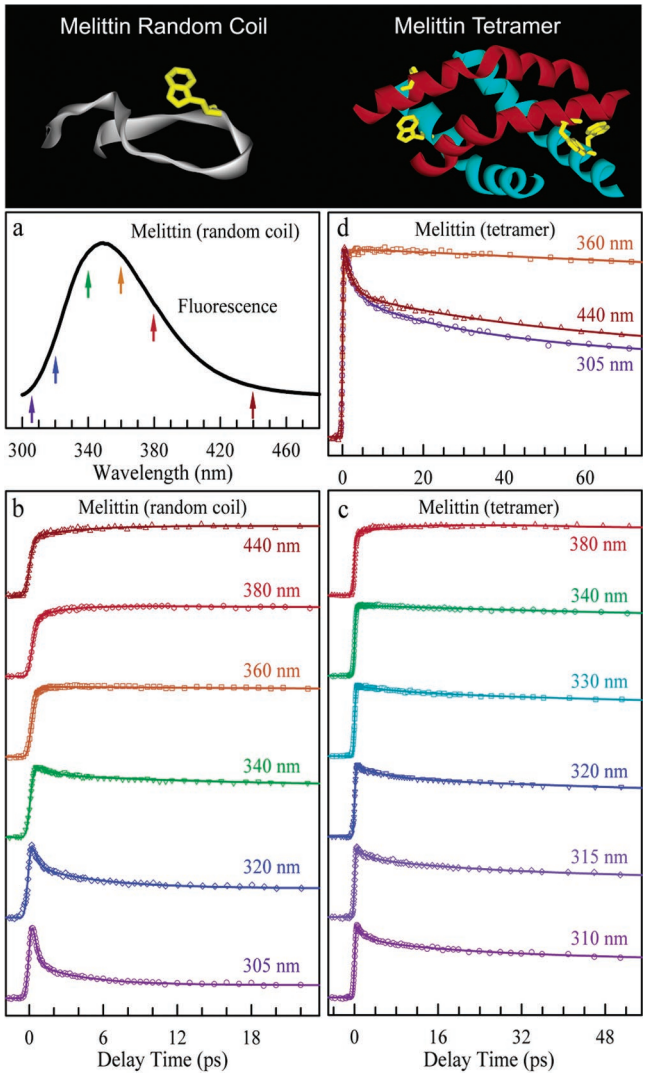

Figure 2. (Top) Melittin monomer in a random-coiled structure from one trajectory MD simulation (800 ps) through melting of the α-helical monomer at 600 K in water (left). X-ray crystallographic structure of melittin tetramer (right).[34] (a) Steady-state fluorescence spectrum of melittin monomer in water. The arrows show typical gated fluorescence wavelengths from the blue to the red side emission. (b) Normalized, femtosecond-resolved transients of melittin monomer with a series of gated fluorescence emissions. Note the systematic changes of transients, decay at the blue side and rise at the red side. (c) Normalized, femtosecond-resolved transients of melittin tetramer with several typical gated fluorescence emissions. (d) Normalized, femtosecond-resolved transients of melittin tetramer with gated far-blue (305 nm), near-red (360 nm), and far-red (440 nm) fluorescence emissions. Note the decay dynamics at 440 nm again, which results from the red-side solvation; see text.

again, a similar temporal behavior to the decay dynamics at the far-blue side of 305 nm, as shown in Figure 2d. We have carefully examined more than 20 proteins we have studied[29] and found similar decay behaviors at the far-red emission (440 nm) as long as the initial solvation response is longer than 1 ps. Moreover, when we gated far more red-side emission (such as 460 nm), the decay time becomes even faster, and the decay amplitude gets even larger. The far red-side decay pattern is simply a mirror image of the blue-side decay transients. This far red-side decay should not be confused with electronic excited-state quenching[30] (see below), since no such fast decay is present in the red-side range of 335−380 nm. Instead, we observed systematic rise components. We attribute the observed new decay dynamics to the red-side solvation. When the initial

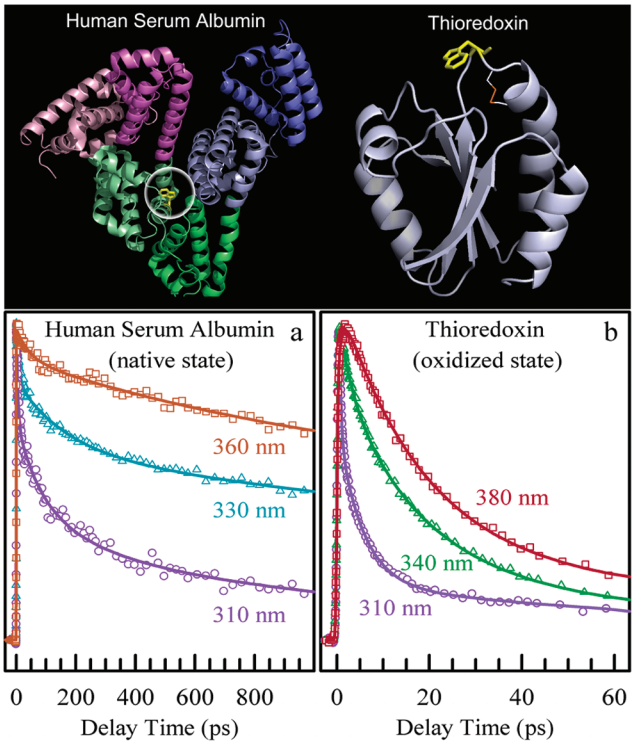

Figure 3. (Top) X-ray crystallographic structures of human serum albumin (left) and human thioredoxin (right). (a) Normalized, femtosecond-resolved transients of human serum albumin in native form with three typical gated fluorescence emissions. Note the *minor* quenching decay component (<15%) of 50 ps at the red-side emissions (360 nm). (b) Normalized, femtosecond-resolved transients of human thioredoxin in oxidized state with three typical gated fluorescence emissions. Note the *dominant* quenching decay component (75%) of 17.6 ps at the red-side emission (380 nm). At the blue side, solvation dynamics is mixed with the quenching process. However, the initial ultrafast relaxation, decay at the blue side and rise at the red side, is still present.

solvation is longer than 1 ps, the excited wave packet has enough time to spread out, and the population quickly "bifurcates", resulting in that some molecules emit and are solvated at the other nuclear turning point, giving longer (far-red) fluorescence emission with ultrafast solvation, which will be discussed in detail below (section C).

B. Electronic Excited-State Quenching. In proteins, excited-state tryptophan fluorescence emission can be quenched mainly by two types of quenchers: protein residues[35] and peptide bonds,[35,36] and prosthetic groups.[10,11] The quenching time scale can range from femtosecond to nanosecond, depending on local structural configuration and quencher properties. For neighboring residues and peptide bonds, the quenching occurs mainly through charge-transfer reactions such as with a disulfide bond, peptide bond, and arginine. For prosthetic groups, the quenching can be through resonance energy transfer with a heme group[10] or ion−sulfur cluster[11] and electron transfer with a flavin cofactor. The studies of these quenching processes themselves are of importance to understanding ultrafast protein dynamics using Trp as a molecular reporter.

Figure 3a shows three typical femtosecond-resolved fluorescence transients of human serum albumin (single Trp214) in the native form at neutral pH with an emission peak at 338 nm. Similar to the melittin results, the two solvation components at the blue side decay in 4.4−9.2 and 104−125 ps, systematically slowing down from 310 nm to the emission peak (338 nm). At the red side from 338 to 380 nm, besides the initial ultrafast rise, we also observed a decay component of 50 ps in all transients, together with systematic decrease in amplitude from

350 nm (15%) to 360 nm (10%) and 370 nm (~0%). The observed 50-ps decay is resulting from the local quenching by a neighboring arginine residue in a 3.81-Å distance (R218).[19,37] This 50-ps component should be present in all transients from the blue to the red side, but it is mixed with the long solvation processes at the blue-side emissions. It should be emphasized that, only using two long lifetimes (1.4 and 6.1 ns) and a 50-ps short quenching lifetime, we cannot globally fit all blue-side transients, and there does exist significantly slow solvation dynamics in 104−125 ps as reported above.[19] Also, the multiple lifetimes, including the ultrafast quenching in tens of picoseconds, do not mean that only several static configurations are present, but directly reflect local conformational flexibility of the protein; the system is in dynamic heterogeneity, mostly occurring on the time scale longer than nanoseconds.

We observed the similar minor quenching (<15% amplitude) at the near red side in many other proteins.[29] One important feature is that the decay time (50 ps in human serum albumin) is the same in all red-side transients (until 380 nm), but the amplitude percentage decreases, consistent with the decay-associated emission spectra (the shorter the lifetime is, the bluer the emission peak, resulting in decrease of percentage contributions when we gated longer fluorescence wavelengths at the red side).[33] Due to the scattering light around 400 nm, we did not attempt to take transients around this region. When we gated the far-red emission at 440 nm, we observed an ultrafast decay component again as we observed in melittin tetramer, a temporal behavior similar to the blue-side decay at 310 nm and a signature of the red-side solvation (see below). Using the same method with or without including the minor quenching component, we obtained the similar solvation correlation functions with a biphasic distribution of 5.0 ps (39%) and 133 ps (61%).[19] The initial solvation response (5 ps) is much longer than 1 ps. Without severe quenching, we still can deduce the time scales of the local solvation dynamics around the tryptophan probe.

With significant quenching of excited-state tryptophan on the ultrafast time scale (<100 ps), tryptophan may not be a good solvation probe, but it could be an excellent reporter for other dynamical processes in proteins. Figure 3b shows three typical femtosecond-resolved fluorescence transients of human thioredoxin in the oxidized state with an emission peak at 339 nm. The single Trp31 is located at the protein surface and mostly exposed to water. In the oxidized state with a disulfide bond (C32−C35) in a 5.75-Å distance,[38] the excited-state tryptophan is expected to be quenched by electron transfer from Trp31 to S−S, leading to a charge separation. At the blue side, all transients show two ultrafast decay components in 0.4−3.1 and 5−17 ps, systematically slowing down from 305 nm to the emission peak (339 nm). At the red side, besides the initial ultrafast rise components in 0.43−0.87 ps, we observed a *dominant* decay component of 17.6 ps in all transients (~75% amplitude). The remaining long-time component (25%) represents some unquenched excited-state population resulting from dynamical conformational heterogeneity.

This observed 17.6 ps is the time scale of electron transfer from Trp* to S−S. Apparently, at the blue side the solvation dynamics is mixed with the electron-transfer quenching. We used the reduced-state protein, where the disulfide bond was reduced to two cysteines and the electron-transfer quenching channel was eliminated, and obtained the solvation dynamics around Trp31 in 0.68 ps (68%) and 13 ps (32%).[31] The second long solvation dynamics (13 ps) is on the same time scale as the electron-transfer quenching (17 ps). Thus, for the oxidized-state protein, we probably obtain the first solvation time scale

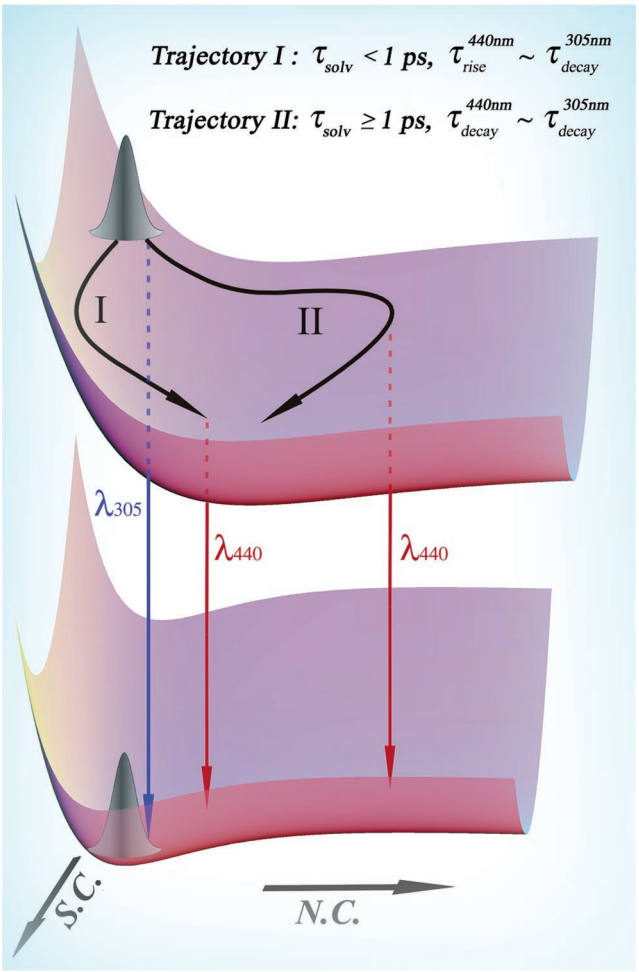

Figure 4. Schematic energy surfaces of ground and excited states along solvation (S.C.) and nuclear (N.C.) coordinates, constructed from harmonic and Morse potentials, respectively. The launched excited-state wave packet ($t = 0$) at nonequilibrium solvation configuration could evolve along two trajectories (I and II), depending on the initial relaxation of local environment. When $\tau_{sol} < 1$ ps, the wave packet moves along trajectory I; while $\tau_{sol} \geq 1$ ps, it first evolves along the nuclear coordinate (trajectory II).

(0.68 ps), but it is not practical to deduce the second long solvation dynamics (13 ps), because both the solvation and quenching processes occur on the same time scale. However, we can obtain the accurate electron-transfer quenching dynamics by femtosecond-resolved fluorescence gating of the relaxed state, typically at the emission peak. Thus, the elucidation of the time scales, in this case, τ_{sol} and τ_{ET} (even $\tau_{sol} \approx \tau_{ET}$), is crucial to the understanding of protein dynamics.

C. Red-Side Solvation and an Internal Clock. In the case of human thioredoxin, the initial solvation response (0.68 ps) is less than 1 ps. We did not observe any ultrafast decay component at the far-red emission (440 nm). Instead, we observed an ultrafast rise component as in random-coiled melittin monomer. With more than 20 proteins we have examined, we did observe ultrafast decay components at the red-end emission (440 nm) when the solvation dynamics is relatively slow and the initial relaxation takes longer than 1 ps. Figure 4 shows two schematic potential surfaces along nuclear and solvation coordinates (N.C. and S.C.) for elucidating the molecular mechanism of the observed solvation dynamics at both the blue- and red-side emissions without severe electronic quenching. The ground and excited states are constructed from a Morse potential with different equilibrium nuclear distances.

The solvation potentials are simply a parabolic function with different equilibrium solvent configurations. Upon excitation, the wave packet is launched at the inner potential turning point in the excited state at a nonequilibrium solvent configuration. The excited-state wave packet will slide down along the solvation coordinate (trajectory I in Figure 4) through local solvent rearrangements as well as spread out along its nuclear coordinate (trajectory II) to the outer potential turning point. The time scale for such spreading along the nuclear coordinate (vibrational periods) is usually less than 1 ps, and the molecules reaching the outer turning point emit at the far-red side (~440 nm) to be formed in the hot ground state. Thus, when the initial solvation response is longer than 1 ps, the wave packet has enough time to move along the nuclear coordinate (trajectory II) and quickly "bifurcates," leading to emission and solvation from both potential turning points and then resulting in a mirror image of the blue- and red-side transient decays as we observed here in melittin tetramer and human serum albumin, and in many other systems.[29] When the initial solvent relaxation is ultrafast on the femtosecond time scale, the wave packet mainly evolves along the solvation coordinate (trajectory I), and the red-side emission results from the relaxed state at the potential well. We will observe ultrafast rise, not decay, components in all red-side transients as we observed here in melittin monomer and human thioredoxin. Thus, the far-red solvation can be taken as an internal clock to evaluate the initial solvation time scale, longer or shorter than 1 ps.

To further validate our proposed molecular mechanism above and to confirm that the observed red-side solvation is only related to the time scale of local environment relaxation, we characterized tryptophan solvation in different water environments. We recently reported[32] water rigidity and ordering around lipidic interfaces in nanochannels (Figure 5, lipidic cubic phase *Pn*3*m* with a 50-Å diameter) and found three types of water (well-ordered, quasi-bound, and bulklike), distributed in about 15 Å from lipid headgroups (Figure 5), using a variable alkyl chain length to systematically anchor tryptophan to different depths of the lipid bilayer and to enable the probe to sample various aqueous environments and examine different layers of water dynamics. All probes, tryptophan alkyl ester molecules, do not exhibit any ultrafast quenching dynamics in the excited state in the lipidic solution. Figure 5 (lower panel) shows a series of transient behaviors from different water environments gated at the far-blue and far-red emissions of 300 and 440 nm.

For tryptophan in bulk water, the initial water relaxation occurs in less than 100 fs;[11,12] thus, we observed initial ultrafast rise components at 440 nm. For tryptophan near the lipidic interface (position 3 in Figure 5), we obtained the initial solvation dynamics in 560 fs. The 300-nm transient shows three decay solvation components of 0.5, 6.1, and 70 ps, and the 440-nm transient has three *rise* components of 0.3, 6.7, and 67 ps. For tryptophan methyl ester located at position 2 (Figure 5), we obtained the initial solvent response in 1.38 ps. At 300 nm, the transient shows three decay solvation components of 0.6, 7.4, and 74 ps, and the 440-nm transient also has three *decay* components of 0.53, 3, and 17 ps. But, at the near red side from the peak emission (338 nm) to 380 nm, we did not observe any decay components and only observed initial rise components. For tryptophan butyl ester buried at position 1 (Figure 5), the initial solvation dynamics obtained occurs in 1.43 ps. Similarly, the 300-nm transient gives three decay solvation components of 0.63, 7.9, and 74 ps and the 440-nm transient also has three decay components of 0.41, 3.1, and 30 ps. The near red-side transients (336−380 nm) all show initial rise components, not decay. Thus, the observed red-side solvation is from the wave packet spreading ("bifurcation") on the femtosecond time scale, and the observed new phenomenon is only related to the time scale of local environment relaxation, independent of local molecular systems. This observation should not be confused with local electronic quenching, and this far red-side solvation is an excellent indicator of local solvation dynamics slower than 1 ps.

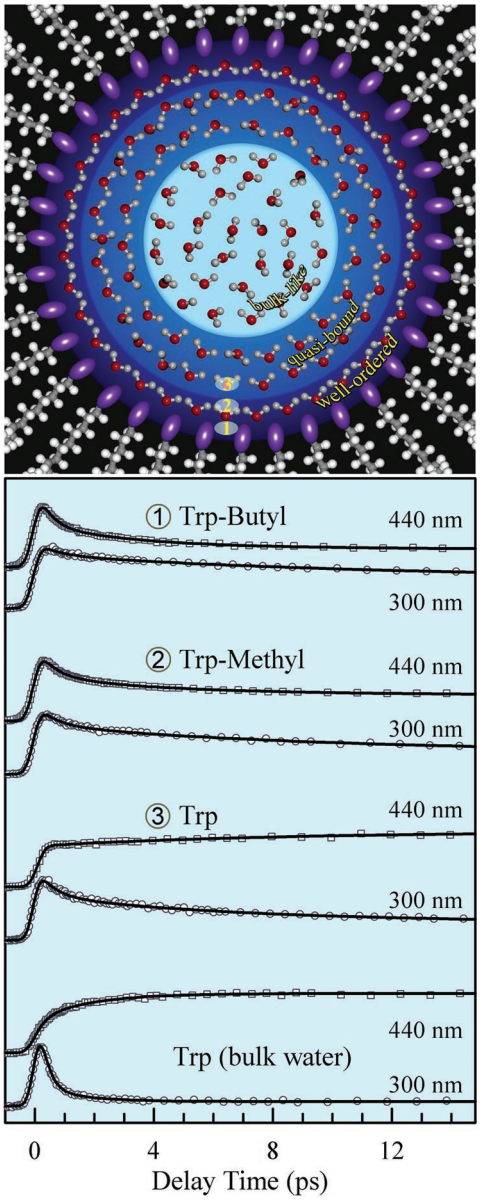

Figure 5. (Upper) Schematic representation of water structures in aqueous nanochannels of ~50 Å in diameter. By anchoring three Trp probes into lipid bilayers, these molecular rulers measure water motions in different local regions in the channel as shown in positions 1−3 of tryptophan butyl ester, tryptophan methyl ester, and tryptophan, respectively. (Lower) Normalized, femtosecond-resolved transients of Trp probes with gated far-blue (300 nm) and far-red (440 nm) fluorescence emissions. Note that, at positions of 1 (well-order water) and 2 (quasi-bound), the transients at 440 nm show *decay* behavior, while at position of 3 (bulklike) and in bulk-free water, the transients at 440 nm initially show *rise* formation.

IV. Conclusion

In this letter, we reported our systematic examination of tryptophan fluorescence dynamics in proteins with femtosecond

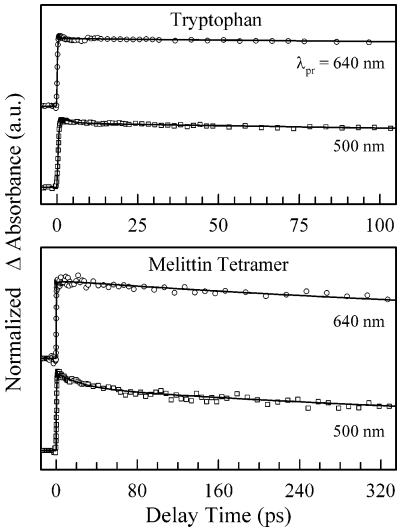

Figure 6. Transient-absorption dynamics of excited tryptophan in water (upper) and melittin tetramer in buffer solution (lower). The pump wavelength is at 290 nm, and probe wavelengths are 640 and 500 nm. The magnitude of all signals is about 7×10^{-4} absorbance change. No significant solvation behaviors were detected, and molecules show nearly constant absorption[39] in the visible region of 480−690 nm during solvation evolution, although a small decay component was observed at the probe wavelength of 500 nm in melittin tetramer.

resolution. Various patterns of femtosecond-resolved fluorescence transients from the blue to the red side have been characterized. Specifically, we can classify tryptophan fluorescence dynamics into three categories: (1) The transients show ultrafast decay at the blue side and rise at the red side in the *entire* emission range. The observed dynamics represent local solvation with the initial response faster than 1 ps. There is no local fast electronic quenching. (2) The transients show similar temporal behaviors as above, but at the far red side (typically 440 nm), the transients show the ultrafast decay again, a mirror image of the blue-side transients. The new phenomenon is from the red-side solvation (Figure 4), and the initial local environmental relaxation is slower than 1 ps. There is still no local fast electronic quenching. (3) The transients show similar dynamical behaviors in the blue-side emission, but all red-side transients have a fast decay with the same time constant and decreasing amplitudes. This fast decay at the red side results from local electronic quenching, and at the blue side, the dynamics is mixed with solvation processes. Depending on the initial solvation response, faster or slower than 1 ps, the transients at the far-red emission have different behaviors, rise or decay, respectively. If local quenching is not severe, the solvation dynamics can still be deduced. If local quenching is significant, we can obtain the accurate quenching dynamics by femtosecond-resolved fluorescence gating of the relaxed state, typically at the emission peak. Thus, tryptophan is an ideal local optical probe for hydration dynamics and protein−water interactions, as shown here in melittin and human serum albumin and at lipid interfaces, as well as an excellent local molecular reporter for ultrafast electron transfer and resonance energy transfer in proteins, as shown here for human thioredoxin. Unlike the transient-absorption method,[39] which shows a constant absorption of excited tryptophan over a wide range of spectrum and is insensitive to solvation processes (Figure 6), the femtosecond-resolved fluorescence studies of tryptophan in proteins using the powerful up-conversion technique will continue to elucidate ultrafast protein dynamics and reveal new molecular mechanisms.

Acknowledgment. This work was supported in part by grants from the Petroleum Research Fund (PRF42734-G4), the National Science Foundation (CHE-0517334), and the Packard Fellowship. We would like to thank Professor David A. R. Sanders (University of Saskatchewan) for providing us human thioredoxin, Professor Martin Caffrey for suggestion of lipid work, and Dr. K. Reildl for lipid sample preparation. Also, thanks to Wenyun Lu and Jongjoo Kim for initial help with experiments and to Jeff Stevens for his thorough reading of the manuscript.

References and Notes

(1) Beechem, J. M.; Brand, L. *Annu. Rev. Biochem.* **1985**, *54*, 43.
(2) Eftink, M. R. In *Methods of Biochemical Analysis*; Suelter, C. H., Ed.; John Wiley & Sons: New York, 1991; Vol. 35.
(3) Lakowicz, J. R. *Principles of Fluorescence Spectroscopy*; Springer: New York, 1999.
(4) *Topics in Fluorescence Spectroscopy, Vol. 6: Protein Fluorescence*; Lakowicz, J. R., Ed.; Kluwer Academic: New York, 2000.
(5) Callis, P. R. *Methods Enzymol.* **1997**, *278*, 113.
(6) Lakowicz, J. R. *Photochem. Photobiol.* **2000**, *72*, 421.
(7) Stubbe, J.; van der Donk, W. A. *Chem. Rev.* **1998**, *98*, 705. Stubbe, J.; Nocera, D. G.; Yee, C. S.; Chang, M. C. Y. *Chem. Rev.* **2003**, *103*, 2167.
(8) Zhong, D.; Zewail, A. H. *Proc. Natl. Acad. Sci. U.S.A.* **2001**, *98*, 11867. Mataga, N.; Chosrowjan, H.; Shibata, Y.; Tanaka, F.; Nishina, Y.; Shiga, K. *J. Phys. Chem. B* **2000**, *104*, 10667. Mataga, N.; Chosrowjan, H.; Taniguchi, S.; Tanaka, F.; Kido, N.; Kitamura, M. *J. Phys. Chem. B* **2002**, *106*, 8917.
(9) Saxena, C.; Sancar, A.; Zhong, D. *J. Phys. Chem. B* **2004**, *108*, 18026. Aubert, C.; Vos, M. H.; Mathis, P.; Eker, A. P. M.; Brettel, K. *Nature (London)* **2000**, *405*, 586. Byrdin, M.; Eker, A. P. M.; Vos, M. H.; Brettel, K. *Proc. Natl. Acad. Sci. U.S.A.* **2003**, *100*, 8676.
(10) Hochstrasser, R. M.; Negus, D. K. *Proc. Natl. Acad. Sci. U.S.A.* **1984**, *81*, 4399. Janes, S. M.; Holtom, G.; Ascenzi, P.; Brunori, M.; Hochstrasser, R. M. *Biophys. J.* **1987**, *51*, 653. Gryczynski, Z.; Tenenholz, T.; Bucci, E. *Biophys. J.* **1992**, *63*, 648.
(11) Zhong, D.; Pal, S. K.; Zhang, D.; Chan, S. I.; Zewail, A. H. *Proc. Natl. Acad. Sci. U.S.A.* **2002**, *99*, 13.
(12) Shen, X.; Knutson, J. R. *J. Phys. Chem. B* **2001**, *105*, 6260.
(13) Szabo, A. G.; Rayner, D. M. *J. Am. Chem. Soc.* **1980**, *102*, 554.
(14) Pal, S. K.; Peon, J.; Bagchi, B.; Zewail, A. H. *J. Phys. Chem. B* **2002**, *106*, 12376. Pal, S. K.; Zewail, A. H. *Chem. Rev.* **2004**, *104*, 2099.
(15) Peon, J.; Pal, S. K.; Zewail, A. H. *Proc. Natl. Acad. Sci. U.S.A.* **2002**, *99*, 10964. Pal, S. K.; Peon, J.; Zewail, A. H. *Proc. Natl. Acad. Sci. U.S.A.* **2002**, *99*, 1763.
(16) Lu, W.; Kim, J.; Qiu, W.; Zhong, D. *Chem. Phys. Lett.* **2004**, *388*, 120.
(17) Lu, W.; Qiu, W.; Kim, J.; Okobiah, O.; Hu, J.; Gokel, G. W.; Zhong, D. *Chem. Phys. Lett.* **2004**, *394*, 415.
(18) Qiu, W.; Zhang, L.; Kao, Y.-T.; Lu, W.; Li, T.; Kim, J.; Sollenberger, G. M.; Wang, L.; Zhong, D. *J. Phys. Chem. B* **2005**, *109*, 16901.
(19) Qiu, W.; Zhang, L.; Okobiah, O.; Yang, Y.; Wang, L.; Zhong, D.; Zewail, A. H. *J. Phys. Chem. B* **2006**, *110*, 10540.
(20) Wüthrich, K. *Angew. Chem., Int. Ed.* **2003**, *42*, 3340.
(21) Mattos, C. *Trends Biochem. Sci.* **2002**, *27*, 203.
(22) Bizzarri, A. R.; Cannistraro, S. *J. Phys. Chem. B* **2002**, *106*, 6617.
(23) Finney, J. L. *Faraday Discuss.* **1996**, *103*, 1. See references therein.
(24) Bryant, R. G. *Annu. Rev. Biophys. Biomol. Struct.* **1996**, *25*, 29.
(25) *Protein−Solvent Interaction*; Gregory, R. B., Ed.; Marcel Dekker: New York, 1995.
(26) Timasheff, S. N. *Annu. Rev. Biophys. Biomol. Struct.* **1993**, *22*, 67.
(27) Teeter, M. M. *Annu. Rev. Biophys. Biophys. Chem.* **1991**, *20*, 577.
(28) Otting, G.; Liepinsh, E.; Wüthrich, K. *Science* **1991**, *254*, 974.
(29) Kao, Y.-T.; Zhong, D. In preparation.
(30) Xu, J.; Toptygin, D.; Graver, K. J.; Albertini, R. A.; Savtchenko, R. S.; Meadow, N. D.; Roseman, S.; Callis, P. R.; Brand, L.; Knutson, J. R. *J. Am. Chem. Soc.* **2006**, *128*, 1214.
(31) Qiu, W.; Zhong, D. In preparation.
(32) Kim, J.; Lu, W.; Qiu, W.; Wang, L.; Caffrey, M.; Zhong, D. *J. Phys. Chem. B* , submitted for publication.

(33) Pan, C.-P.; Callis, P. R.; Barkley, M. D. *J. Phys. Chem. B* **2006**, *110*, 7009.

(34) Terwilliger, T. C.; Eisenberg, D. *J. Biol. Chem.* **1982**, *257*, 6010. Terwilliger, T. C.; Eisenberg, D. *J. Biol. Chem.* **1982**, *257*, 6016.

(35) Chen, Y.; Liu, B.; Yu, H.-T.; Barkley, M. D. *J. Am. Chem. Soc*. **1996**, *118*, 9271. Chen, Y.; Barkley, M. D. *Biochemistry* **1998**, *37*, 9976.

(36) Callis, P. R.; Liu, T. *J. Phys. Chem. B* **2004**, *108*, 4248. Callis, P. R.; Vivian, J. T. *Chem. Phys. Lett.* **2003**, 369, 409.

(37) (a) Siemiarczuk, A.; Petersen, C. E.; Ha, C.-E.; Yang, J.; Bhagavan, N. V. *Cell Biochem. Biophys.* **2004**, *40*, 115. (b) Wardell, M.; Wang, Z.; Ho, J. X.; Robert, J.; Ruker, F.; Ruble, J.; Carter, D. C. *Biochem. Biophys. Res. Commun.* **2002**, *291*, 813. Carter, D. C.; Ho, J. X. *Adv. Protein Chem.* **1994**, *45*, 153. He, X. M.; Carter, D. C. *Nature (London)* **1992**, *358*, 209.

(38) Weichsel, A.; Gasdaska, J. R.; Powis, G.; Montfort, W. R. *Structure* **1996**, *4*, 735.

(39) Peon, J.; Hess, G. C.; Pecourt, J.-M. L.; Yuzawa, T.; Kohler, B. *J. Phys. Chem. A* **1999**, *103*, 2460.